Hindawi
Modelling and Simulation in Engineering
Volume 2021, Article ID 6688806, 13 pages
https://doi.org/10.1155/2021/6688806

Research Article

Solving Parabolic and Hyperbolic Equations with Variable Coefficients Using Space-Time Localized Radial Basis Function Collocation Method

Mohammed Hamaidi,[1] **Ahmed Naji**,[1] **and Ahmed Taik**[2]

[1]*Department of Mathematics, Faculty of Sciences and Techniques, Abdelmalek Essaâdi University, Box 416, Tangier, Morocco*
[2]*Laboratory Mathematics & Applications, Department of Mathematics, FSTM, University Hassan II Casablanca, Morocco*

Correspondence should be addressed to Mohammed Hamaidi; hamaidi@yahoo.com

Received 21 October 2020; Revised 4 January 2021; Accepted 17 January 2021; Published 8 February 2021

Academic Editor: Luis Carlos Rabelo

In this paper, we investigate the numerical approximation solution of parabolic and hyperbolic equations with variable coefficients and different boundary conditions using the space-time localized collocation method based on the radial basis function. The method is based on transforming the original d-dimensional problem in space into $(d+1)$-dimensional one in the space-time domain by combining the d-dimensional vector space variable and 1-dimensional time variable in one $(d+1)$-dimensional variable vector. The advantages of such formulation are (i) time discretization as implicit, explicit, θ-method, method-of-line approach, and others are not applied; (ii) the time stability analysis is not discussed; and (iii) recomputation of the resulting matrix at each time level as done for other methods for solving partial differential equations (PDEs) with variable coefficients is avoided and the matrix is computed once. Two different formulations of the d-dimensional problem as a $(d+1)$-dimensional space-time one are discussed based on the type of PDEs considered. The localized radial basis function meshless method is applied to seek for the numerical solution. Different examples in two and three-dimensional space are solved to show the accuracy of such method. Different types of boundary conditions, Neumann and Dirichlet, are also considered for parabolic and hyperbolic equations to show the sensibility of the method in respect to boundary conditions. A comparison to the fourth-order Runge-Kutta method is also investigated.

1. Introduction

Second-order parabolic and hyperbolic partial differential equations with variable coefficients are one of the most important problems in Mathematical and engineering fields. They attract the attention of a large number of scientists. The general heat transfer problem is considered one of the more interesting examples. Such initial boundary value problems (parabolic or hyperbolic) can be solved by coupling time-stepping algorithms with different numerical methods such as finite element, finite volume, boundary elements methods, meshless methods, fundamental solutions, and spectral and wavelet methods. In [1], Parzlivand and Shahrezaee presented a numerical technique based on a combination of collocation method and radial basis functions to solve parabolic partial differential equations with time-dependent coefficients. Dehghan and Shokri [2] have employed the thin-plate splines RBFs in the collocation RBF method to solve the two-space dimensional linear hyperbolic equation with variable coefficients, subject to appropriate initial and Dirichlet boundary conditions. A new version of the method of approximate particular solutions using radial basis functions has been proposed in [3] by Jiang et al. for solving elliptic partial differential equations with variable coefficients. In this paper [3], a comparison to Kansa's method and the method of fundamental solutions has also been investigated. Some other investigation of meshless methods to PDEs with variable coefficients is given in [4–6]. We can also mention the works of Gu et al. [7, 8], where they used local versions of meshless methods leading to sparse matrices.

In most published works, these methods are based on first discretizing the time variable by applying any time

time-stepping algorithms as implicit, explicit, Runge-Kutta, or others; and seeking the approximate solution at each instant t in a space domain problem.

The space-time methods have seen some investigation these last decades. Among them, we can mention the space-time finite element method developed by Tayfun et al. in [9] for the computation of fluid-structure interaction problems. Klaij et al. have also developed the space-time discontinuous Galerkin finite element method for solving compressible Navier-Stokes equations in [10] and advection-diffusion problems in [11]. The technique has also been applied to shallow water flows by Ambati et al. in [12].

Although few works were published concerning the space-time meshless method for solving PDEs with independent variable coefficients [13–18], up to date and to our best knowledge, there is no investigation on the application of space-time meshless method for solving PDEs with either variable or time-dependent variable coefficients. In this paper, we investigate the application of space-time localized meshless collocation radial basis functions developed in [13] to a general second-order parabolic and hyperbolic problems, with variable coefficients.

The method is based on firstly transforming the considered d-dimensional evolutionary problem in space as a $(d+1)$-dimensional space-time one. The formulation starts by combining the d-dimensional vector space variable and 1-dimensional time variable in one $(d+1)$-dimensional variable vector and defining the space-time domain and its boundary. Then, the boundary conditions are sited on the global space-time boundary domain for PDEs with the first derivative with respect to time and on just one part of the boundary for PDEs with the second derivative with respect to time. The method does not need first to discretize all derivatives with respect to time and solve the problem in the space domain at each time level, as it is usually the case with many numerical methods. The developed formulation leads always to a square algebraic resulting system and benefit from the following advantages:

(i) The time stability analysis is not discussed as it is the case for other time-stepping schemes as implicit, explicit, θ-method, etc.

(ii) Reducing the computational time as there is no need to recompute the matrix for the resulting algebraic system at each time level, unlike the case for others time integration methods used to solve PDEs with time-dependent coefficients

(iii) Solving hyperbolic partial differential equations with variable coefficients as inverse problem, since just the hyperbolic equation with constant coefficients is less discussed in the literature and needs more sophisticated time integration technique

The paper is organized as follows. In Section 2, we introduce the formulation of the parabolic and hyperbolic problem as space-time problem and the space-time localized RBF method implementation. Section 3 is devoted to the discussion of results obtained by solving different parabolic and hyperbolic examples in two- and three-dimensions in regular and irregular domains. A comparison of the given technique to the fourth-order Runge-Kutta method is also given in Section 4. We conclude in Section 5.

2. Space-Time Localized RBF Method Formulation

To recall the space-time localized RBF method defined in [13], let $\Omega \subset \mathbb{R}^d$ be a bounded domain with a sufficiently regular boundary $\partial\Omega$ and consider the following time-dependent boundary value problem

$$\frac{\partial}{\partial t}u(x,t) + \mathscr{P}_{(x,t)}u(x,t) = f(x,t) \forall x \in \Omega, \forall t \in]0,T], \tag{1}$$

$$\mathscr{B}u(x,t) = g(x,t) \forall x \in \partial\Omega, \forall t \in]0,T[, \tag{2}$$

$$u(x,0) = u_0(x) \forall x \in \Omega, \tag{3}$$

or

$$\frac{\partial^2}{\partial t^2}u(x,t) + \mathscr{P}_{(x,t)}u(x,t) = f(x,t) \forall x \in \Omega, \forall t \in]0,T], \tag{4}$$

$$\mathscr{B}u(x,t) = g(x,t) \forall x \in \partial\Omega, \forall t \in]0,T[, \tag{5}$$

$$u(x,0) = u_0(x) \forall x \in \Omega, \tag{6}$$

$$\frac{\partial}{\partial t}u(x,0) = u_1(x) \forall x \in \Omega, \tag{7}$$

where $\mathscr{P}(x,t)$ is a differential operator of second order with variable coefficients of the form:

$$\mathscr{P}_{(x,t)}u = \sum_{i=1}^{i=d}\sum_{j=1}^{j=d} a(x,t)\frac{\partial^2 u}{\partial x_i \partial x_j} + b(x,t)u, \tag{8}$$

and $\mathscr{B}$ is a linear boundary operator depending on the kind of problem treated. The given functions f, g, u_0, and u_1 are assumed to be sufficiently regular.

The formulation of the evolutionary problems given by (1-2-3) and (4-5-6-7) as a space-time one starts by combining the space variable x and the time variable t in one $(d+1)$-dimensional vector. The constructed variable vector belongs to the space-time domain $\Omega_T = \Omega \times]0,T[$ represented by Figure 1 for some simple cases. The boundary of the new formulated domain Ω_T is given by $\partial\Omega_T = \Omega \times \{t = T\}, \partial\Omega \times [0,T], \Omega \times \{t = 0\}$.

As discussed in [13], the formulation of the d-dimensional problem as a $(d+1)$-dimensional space-time one depends on the type of equations considered. For the problem given by Eqs. (1)–(3), Eq. (1) given by $(\partial/\partial t)u + \mathscr{P}_{(x,t)}u = f(x,t)$, $\forall (x,t) \in \Omega \times]0,T[$ is considered as a domain equation in Ω_T and Eqs. (2) and (3) as boundary conditions on $\partial\Omega \times [0,T]$ and $\Omega \times \{t = 0\}$, respectively. To complete the set of boundary conditions on the $\partial\Omega_T$, we define Eq. (1) as a

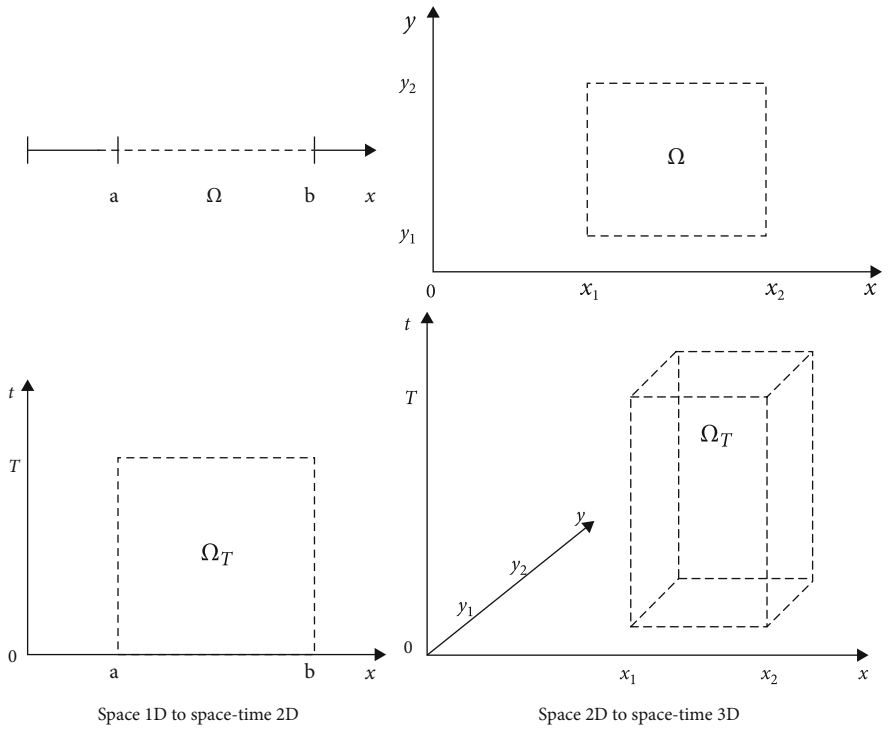

Figure 1: Space-time domain concept.

boundary condition on $\Omega \times \{t = T\}$. The formulation is completed, and the new form of the system is

$$\frac{\partial}{\partial t} u(x,t) + \mathscr{P}_{(x,t)} u(x,t) = f(x,t) \forall (x,t) \in \Omega_T, \tag{9}$$

$$\frac{\partial}{\partial t} u(x,t) + \mathscr{P}_{(x,t)} u(x,t) = f(x,t) \forall (x,t) \in \Omega \times \{t = T\}, \tag{10}$$

$$\mathscr{B} u(x,t) = g(x,t) \forall x \in \partial\Omega, \times]0, T[, \tag{11}$$

$$u(x,t) = u_0(x) \forall x \in \Omega \times \{t = 0\}. \tag{12}$$

For the case of the hyperbolic equation, we do not need any boundary condition on the part on the part of the space-time boundary characterized by $\Omega \times \{t = T\}$. The problem is solved as an ill-posed one, and the algebraic system is square (see [1]).

Then, the system has the new form:

$$\frac{\partial^2}{\partial t^2} u(x,t) + \mathscr{P}_{(x,t)} u(x,t) = f(x,t) \forall (x,t) \in \Omega_T, \tag{13}$$

$$\frac{\partial}{\partial t} u(x,t) = u_1(x) \forall x \in \Omega \times \{t = 0\}, \tag{14}$$

$$\mathscr{B} u(x,t) = g(x,t) \forall x \in \partial\Omega, \times]0, T[, \tag{15}$$

$$u(x,t) = u_0(x) \forall x \in \Omega \times \{t = 0\}. \tag{16}$$

Figure 2 summarizes the defined space-time problems for the two considered cases.

In general, to construct the approximate solution of this news system, we select a number of distinct centers points $\{\widehat{x}_j = (x_j, t_j)\}_{j=1}^{Ni}$ and $\{\widehat{x}_j = (x_j, t_j)\}_{j=Ni+1}^{N}$ in the domain Ω_T and on its boundary $\partial\Omega_T$, respectively. The finite-dimensional space V_Φ that contains the RBF interpolation functions is defined by

$$V_\Phi = \operatorname{span}\{\Phi(\|.-\widehat{x}_1\|), \Phi(\|.-\widehat{x}_2\|), \cdots, \Phi(\|.-\widehat{x}_N\|)\} + \mathbb{P}_m^{d+1}, \tag{17}$$

where m is the order of the used conditionally positive defined function Φ. The approximate function is given by

$$s_V(\widehat{x}) = s_V(x,t) = \sum_{j=1}^{N} \alpha_j \Phi_j(\widehat{x}). \tag{18}$$

We can mention that the space-time domain $\Omega_T = \Omega \times]0, T[$ satisfies the interior cone condition since the domain Ω and the interval $]0, T[$ are also satisfying the interior cone condition. So, the lemma of error interpolation cited in [19] is satisfied for the case of the space-time domain (see also [13]).

The general form of the system of Eqs. (9)–(12) or (13)–(16) can be written under the following form:

$$\begin{aligned} \mathbf{L}_{\widehat{x}} u(\widehat{x}) &= f(\widehat{x}) \quad \forall \widehat{x} \in \Omega_T, \\ \mathbf{B}_{\widehat{x}} u(\widehat{x}) &= h(\widehat{x}) \quad \forall \widehat{x} \in \partial\Omega_T, \end{aligned} \tag{19}$$

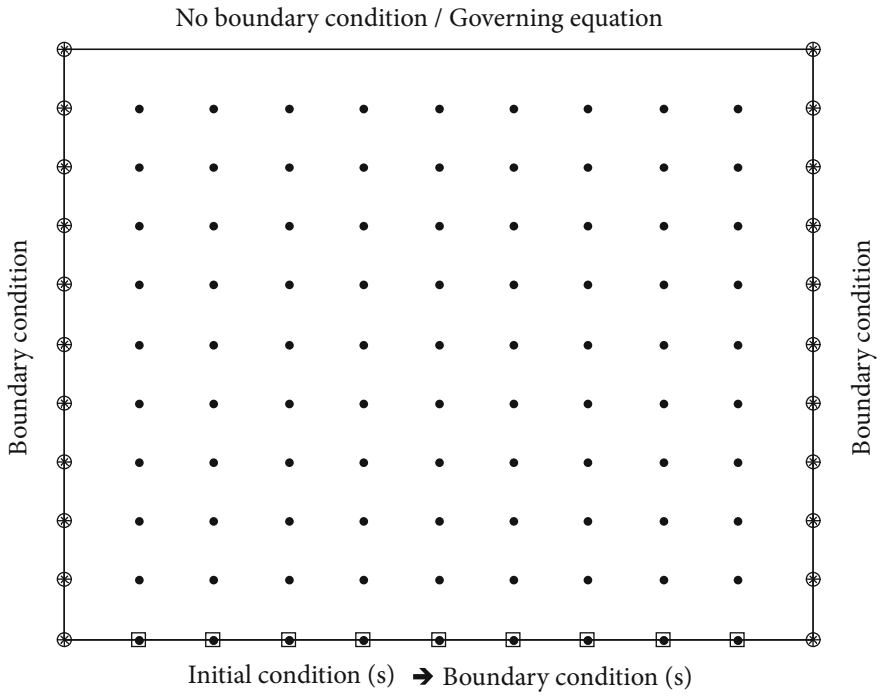

Figure 2: Domain of space-time formulation.

where $\mathbf{L}_{\hat{x}} = \partial/\partial t + \mathscr{P}_{(x,t)}$ on Ω_T, $\mathbf{B}_{\hat{x}} = [\mathbf{L}_{\hat{x}} \quad \mathscr{B} \quad \mathbf{1}]$ and $h = [f \quad g \quad u_0]^t$ on $\partial\Omega_T$ for the parabolic case and $\mathbf{L}_{\hat{x}} = \partial^2/\partial t^2 + \mathscr{P}_{(x,t)}$ on Ω_T, $\mathbf{B}_{\hat{x}} = [\partial/\partial t \quad \mathscr{B} \quad \mathbf{1}]$ and $h = [u_1 \quad g \quad u_0]^t$ on $\partial\Omega_T$ for the hyperbolic case.

Following Li et al. [20] and by Yao et al. [21], a localized influence domain Ω_T^s for each point $\hat{x}_s \in \Omega_T$ is selected. It contains a number n_s of neighboring points $\{\hat{x}_k^{[s]}\}_{k=1}^{n_s} \in \Omega_T^s$ to the selected center $\hat{x}_s$. (see Figure 3). Then, the proximate function in the subdomain Ω_T^s is given by the expansion

$$u(\hat{x}_s) \simeq \hat{u}(\hat{x}_s) = \sum_{k=1}^{n_s} \alpha_k \Phi\left(\|\hat{x}_s - \hat{x}_k^{[s]}\|\right), \tag{20}$$

where $\{\alpha_k\}_{k=1}^{n_s}$ are the unknown coefficients, $\|\cdot\|$ is the Euclidean norm, and Φ is the chosen RBF.

Applying Eq. (20) to $\{\hat{x}_k^{[s]}\}_{k=1}^{n_s} \subset \Omega_T^s$ set points, we get $n_s \times n_s$ linear equations given by

$$\hat{\mathbf{u}}^{[s]} = \mathbf{\Phi}^{[s]} \boldsymbol{\alpha}^{[s]}, \tag{21}$$

where $\mathbf{\Phi}^{[s]} = [\Phi(\|\hat{x}_i^{[s]} - \hat{x}_j^{[s]}\|)]_{1 \le i,j \le n_s}$.

Then, the problem of seeking the expansion coefficients $\{\alpha_k\}_{k=1}^{n_s}$ is transformed into a determination of the values of the solution $\hat{u}$ at each center points $\{\hat{x}_k^{[s]}\}_{k=1}^{n_s} \subset \Omega_T^s$ by using the equation

$$\boldsymbol{\alpha}^{[s]} = \left(\mathbf{\Phi}^{[s]}\right)^{-1} \hat{\mathbf{u}}^{[s]}. \tag{22}$$

For $\hat{x}_s \in \Omega_T^s$, we apply the differential operator $\mathbf{L}_{\hat{x}}$ to Eq. (20) to obtain the following equation

$$\mathbf{L}_{\hat{x}} \hat{u}(\hat{x}_s) = \sum_{k=1}^{n_s} \alpha_k L_{\hat{x}} \Phi\left(\|\hat{x}_s - \hat{x}_k^{[s]}\|\right) = \mathbf{Y}^{[s]} \hat{\mathbf{u}}^{[s]}, \tag{23}$$

where $\hat{\mathbf{u}}^{[s]} = [u(\hat{x}_1^s), u(\hat{x}_2^s), \cdots, u(\hat{x}_{n_s}^s)]$ and $\mathbf{Y}^{[s]} = \mathbf{L}_{\hat{x}} \mathbf{\Phi}^{[s]} \left(\mathbf{\Phi}^{[s]}\right)^{-1}$. The vector $\hat{\mathbf{u}} = [u(\hat{x}_1), u(\hat{x}_2), \cdots, u(\hat{x}_N)]$ is incorporated in the system of (23) by adding zeros at the proper locations based on the mapping of $\hat{\mathbf{u}}^{[s]}$ to $\hat{\mathbf{u}}$, and considering the $\mathbf{Y}_{1\times N}$ as the global expansion of $\mathbf{Y}_{1\times n_s}^{[s]}$. The global system of Eq. (23) is then written under the form

$$f(\hat{x}_s) = \mathbf{L}_{\hat{x}} \hat{u}(\hat{x}_s) = \mathbf{Y}(\hat{x}_s) \hat{\mathbf{u}}. \tag{24}$$

In the same way, selecting a center $\hat{x}_s$ on the boundary $\partial\Omega_T$, we have

$$\mathbf{B}_{\hat{x}} u(\hat{x}_s) = \sum_{k=1}^{n_s} \alpha_k \mathbf{B}_{\hat{x}} \Phi\left(\|\hat{x}_s - \hat{x}_k^{[s]}\|\right) = \mathbf{\Theta}^{[s]} \hat{\mathbf{u}}, \tag{25}$$

where $\mathbf{\Theta}^s = \mathbf{B}_{\hat{x}} \mathbf{\Phi}^{[s]} \left(\mathbf{\Phi}^{[s]}\right)^{-1}$. In a global form, the system is then written as

$$h(\hat{x}_s) = \mathbf{B} \hat{u}(\hat{x}_s) = \mathbf{\Theta}(\hat{x}_s) \hat{\mathbf{u}}, \tag{26}$$

where $\mathbf{\Theta}$ is the expansion of $\mathbf{\Theta}^{[s]}$ by adding zeros.

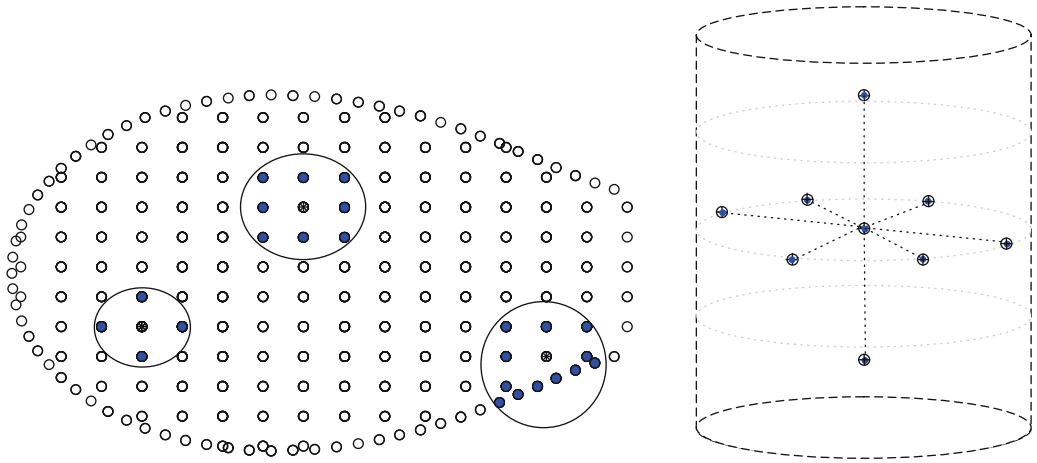

Figure 3: Schematic showing five-node, nine-node, and thirteen-node local domains Ω_s for 2D (left) and nine-node local domain for 3D (right).

By collocating at all centers points $\{\widehat{x}_j\}_{j=1}^{N}$ using Eqs. (24) and (26), we get the following sparse linear system of equations

$$\begin{bmatrix} Y \\ \Theta \end{bmatrix} \begin{bmatrix} \widehat{u} \\ \end{bmatrix} = \begin{bmatrix} f \\ h \end{bmatrix}, \tag{27}$$

where

$$Y = \begin{bmatrix} Y(\widehat{x}_1) \\ .. \\ .. \\ Y(\widehat{x}_{Ni}) \end{bmatrix} \quad \text{and} \quad \Theta = \begin{bmatrix} \Theta(\widehat{x}_{Ni+1}) \\ .. \\ .. \\ \Theta(\widehat{x}_N) \end{bmatrix}. \tag{28}$$

The approximate solution at the interpolation points $\{\widehat{V}(\widehat{x}_j)\}_{j=1}^{N}$ can be obtained by solving the above sparse linear system of equations.

3. Numerical Simulations

The investigated test examples in this section are two- and three-dimensional parabolic and hyperbolic equations with variable coefficients given as follows:

$$\frac{\partial u}{\partial t} + a(\mathrm{x}, t)\Delta u + b(x, t)u = f \text{ in } \Omega \times (0, T], \tag{29}$$

$$\frac{\partial^2 u}{\partial t^2} + a(x, t)\Delta u + b(x, t)u = f \text{ in } \Omega \times (0, T]. \tag{30}$$

Knowing the shape of the space-time domain Ω_T, the distributed nodes can be done uniformly or randomly without making any distinction between space and time variables. Through these numerical simulations, n_s denotes the number of neighboring points in an influence space-time domain Ω_T. To balance between the approximation quality of PDEs solution and sparsity of the algebraic matrix, a reasonable value of n_s is chosen to be at least 2 dim $(\Omega_T) + 1$ when dealing with Dirichlet boundary condition. More points can be added in the case of the Neumann condition depending the on problem treated (see [13] for more details). Seeking optimal values of shape parameter is still an open subject in the area of numerical approximation of PDEs. Many techniques have been proposed in the literature without any theoretical analysis. The $N = (N_d + N_b) \times N_t$ is the total number of nodes used, where N_b and N_d are the number of boundary and interior nodes of space domain Ω, respectively, and N_t is the number of nodes on the time axe which can be either uniform or random.

In all proposed simulations, Neumann and Dirichlet boundary conditions are considered for parabolic and hyperbolic equations to show the sensibility of the method in respect to different boundary conditions on the space domain. Although any RBF can be used to test the technique, the multiquadric radial basis function (MQ) is the function used for all given simulations. The MQ-RBF is defined by $\Phi(r) = \sqrt{1 + \varepsilon^2 r^2}$, where ε is the shape parameter and r is the distance between two nodes.

The validity and the accuracy of the presented technique are demonstrated by considering the following discrete error-norms; the maximum absolute error (MAE), the root mean squared error (RMSE), and the L_{er}^1 relative errors are defined by

$$\mathrm{MAE} = \max_{1 \le j \le N} \left|\widehat{u}_j - u_j\right|, \quad \mathrm{RMSE} = \sqrt{\frac{1}{N}\sum_{j=1}^{N}\left(\widehat{u}_j - u_j\right)^2}, \quad L_{er}^1 = \frac{\sum_{j=1}^{N}\left|\widehat{u}_j - u_j\right|}{\sum_{j=1}^{N}\left|u_j\right|}, \tag{31}$$

where u_j and $\widehat{u}_j$ are the exact and the approximate solutions at (x_j, t_j), respectively.

Table 1: Comparison of numerical results obtained using space-time method (top) and RK4 method (bottom).

T	0.1	0.2	0.5	1	1
			Space-time		
N_t	20	20	20	20	40
CPU time	0.07231	0.06717	0.06657	0.06844	0.18470
MAE	8.80E-04	1.59E-03	3.22E-03	1.02E-03	8.63E-04
RMSE	5.96E-04	1.12E-03	2.29E-03	7.31E-04	6.16E-04
			RK4 method		
dt	0.001	0.001	0.001	0.001	0.0005
CPU time	1.68775	2.92439	7.51148	13.71638	27.19279
MAE	3.95E-03	4.63E-03	5.72E-03	—	2.72E-03
RMSE	1.42E-03	1.83E-03	2.50E-03	—	6.92E-04

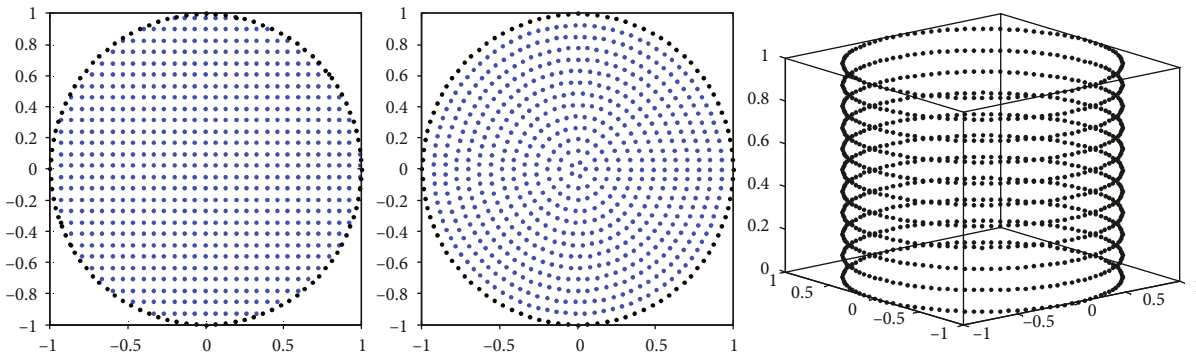

Figure 4: Uniform and circular distributions of nodes for the 2D space domain and the 3D space-time domain.

3.1. One-Dimensional Test and Comparison with Runge-Kutta Method. To show the efficiency of the space-time method in word of stability and CPU time, we compare it to the 4th order Runge-Kutta method. The investigated example is the one-dimensional convection-diffusion PDE with variable coefficients defined as follows:

$$\frac{\partial u}{\partial t} - (x+t)\frac{\partial^2 u}{\partial x^2} + (2x+3t)\frac{\partial u}{\partial x} = 0. \tag{32}$$

The initial and the boundary conditions are defined according to the analytical solution given by $u(x,t) = \exp(2x - t^2)$, and the space domain is $\Omega = [0,1]$.

As the coefficients are depending on t, the matrix construction is called 4 times at each time step using the 4th order Runge-Kutta method, which enlarges the CPU time. According to Table 1, the CPU computation time of the Runge-Kutta method is much larger than that of the space-time technique. We can also mention that time stability is not guaranteed in the Runge-Kutta method or any other time-stepping algorithms. Besides the implementation simplicity of the demonstrated technique, results show that our method is faster and more accurate than the used Runge-Kutta method.

Table 1 shows that the space-time method is stable and accurate compared to the RK4 method. The space-time method converges for different values of the final time T, keeping the same value of N_t. From the same Table 1, it can be remarked that the RK4 method diverges for the simulation with $T = 1$ and $dt = 0.001$, which means that a smaller value of dt is needed to get the convergence. Regarding to the Table 1 and incase the results of the space-time method is discussed according to dt, we can remark that dt is ranged from 0.05 to 0.025 and results still more accurate. All results are obtained using the same number of nodes on the space domain $N_x = 20$ and the final time T ranges from 0.1 to 1. The shape parameter of the MQ-RBF is chosen to be $\varepsilon = 0.1$.

3.2. Two-Dimensional Parabolic Equations. For examples treated herein, we consider the considered as computation space domain Ω, a two-planar domain given by $\Omega = \{(x,y) \in \mathbb{R}^2 : \|(x,y)\| \leq 1\}$. Two different distributions of nodes, uniform and circular, illustrated in Figure 4, are considered. For uniform distribution of nodes, we take $N_d = 326$ and $N_b = 50$ and $N_d = 320$ and $N_b = 50$ for circular one.

Example 1. As a first simulation, we consider the parabolic example with the analytical solution given by

$$u(x,y,t) = \sin(x+y)\exp(-t),\ (x,t) \in \Omega \times [0,1] \tag{33}$$

where $a(x,y,t) = 1/1 + x^2 + y^2$ and $b(x,y,t) = (x+2)(y+2)$.

Table 2: Results for different values of ε in Example 1 with $N_t = 10$. Uniformly distributed nodes (left) and circular distributed nodes (right), with Dirichlet conditions.

ε	MAE	RMSE	L_{er}^1	MAE	RMSE	L_{er}^1
0.1	1.61E-04	5.60E-05	1.14E-04	3.70E-04	1.21E-04	2.50E-04
0.2	1.44E-04	5.03E-05	1.02E-04	3.38E-04	1.10E-04	2.28E-04
0.3	1.15E-04	4.07E-05	8.46E-05	2.84E-04	9.25E-05	1.91E-04
0.4	7.25E-05	2.78E-05	5.91E-05	2.07E-04	6.72E-05	1.39E-04
0.5	9.80E-05	1.91E-05	2.80E-05	1.11E-04	3.64E-05	7.69E-05
0.6	1.57E-04	3.65E-05	6.99E-05	1.45E-04	3.37E-05	6.10E-05
0.7	2.33E-04	7.19E-05	1.49E-04	2.42E-04	8.56E-05	1.76E-04

Table 3: Results for different values of ε in Example 1 with $N_t = 20$. Uniform spaced nodes (left) and circular nodes (right), using Dirichlet conditions.

ε	MAE	RMSE	L_{er}^1	MAE	RMSE	L_{er}^1
0.1	7.80E-05	2.78E-05	6.04E-05	3.08E-04	9.59E-05	2.03E-04
0.2	6.70E-05	1.93E-05	4.17E-05	2.68E-04	8.22E-05	1.73E-04
0.3	6.37E-05	7.79E-06	1.33E-05	2.04E-04	5.94E-05	1.23E-04
0.4	5.91E-05	2.18E-05	4.94E-05	1.25E-04	2.91E-05	5.80E-05
0.5	1.44E-04	5.19E-05	1.15E-04	1.03E-04	3.10E-05	6.78E-05
0.6	2.58E-04	9.19E-05	2.02E-04	2.28E-04	8.58E-05	1.89E-04
0.7	4.04E-04	1.43E-04	3.12E-04	4.29E-04	1.59E-04	3.51E-04

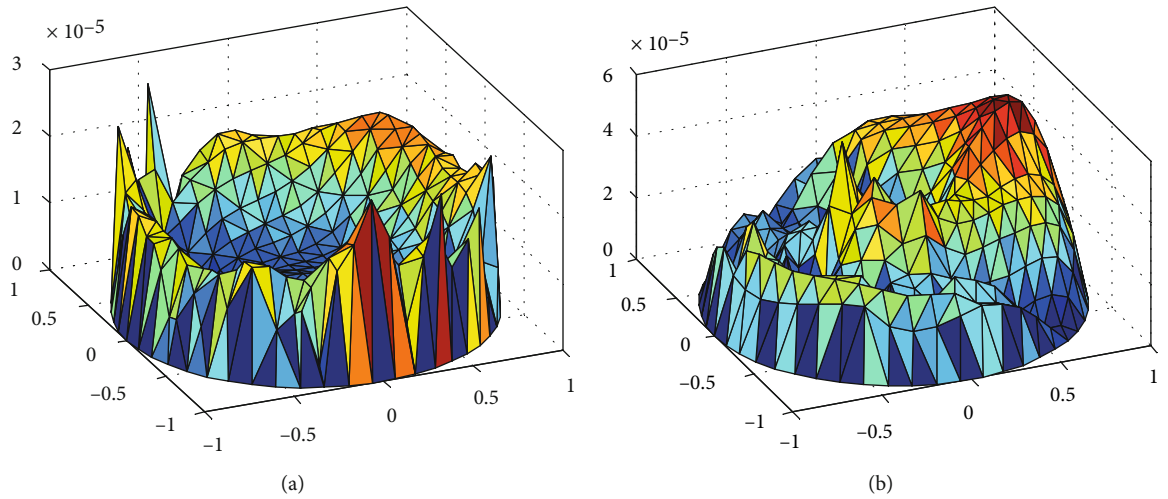

Figure 5: Absolute errors at $t = 1$ with $N_t = 10$. Uniform (a) and circular (b). Example 1 using Dirichlet conditions.

The problem was solved using different values of both N_t and shape parameter ε. Considering Dirichlet boundary condition on $\partial\Omega$, Tables 2 and 3 illustrate results for $N_t = 10$ and $N_t = 20$, respectively. They also show the influence of shape parameter ε on the approximate solution. Using $\varepsilon = 0.25$ and $\varepsilon = 0.43$ for uniform and circular distributions of nodes, respectively, Figure 5 shows the absolute error of the approximate solution at $t = 1$ on the computation space-domain Ω for Dirichlet boundary condition on $\partial\Omega \times [0, T]$. Using uniform distribution of nodes, the obtained maximum absolute error and the root mean square error are MAE $= 2.71 \times 10^{-5}$ and RMSE $= 1.09 \times 10^{-5}$, respectively. For the circular distributed nodes, we obtained MAE $= 5.47 \times 10^{-5}$ and RMSE $= 2.37 \times 10^{-5}$. As the $\Omega_T \subset \mathbb{R}^3$ and the boundary condition are Dirichlet type, the used value of the number of neighboring points is $n_s = 7$.

To demonstrate the influence of the boundary condition on the approximate solution and then on the technique, mixed Neumann-Dirichlet boundary condition is considered on $\partial\Omega$. Dirichlet condition was used on the part of the space domain boundary defined by $\Gamma_1 = \{(x, y) \in \partial\Omega,\ y > 0\}$ and Neumann condition on the other part $\Gamma_2 = \partial\Omega - \Gamma_1$. For this

Table 4: Results for different values of ε in Example 1 with $N_t = 10$. Uniform spaced nodes (left) and circular nodes (right), using Dirichlet and Neumann conditions.

ε	MAE	RMSE	L_{er}^1	MAE	RMSE	L_{er}^1
0.1	4.41E-04	1.13E-04	2.28E-04	3.89E-04	1.58E-04	3.63E-04
0.2	4.18E-04	1.04E-04	2.09E-04	3.79E-04	1.46E-04	3.33E-04
0.3	3.79E-04	8.98E-05	1.77E-04	3.67E-04	1.26E-04	2.83E-04
0.4	3.22E-04	6.90E-05	1.32E-04	3.84E-04	9.96E-05	2.15E-04
0.5	2.45E-04	4.52E-05	7.97E-05	4.05E-04	7.71E-05	1.48E-04
0.6	1.61E-04	4.20E-05	8.33E-05	4.26E-04	8.79E-05	1.68E-04
0.7	2.73E-04	8.41E-05	1.82E-04	4.61E-04	1.47E-04	3.09E-04

Table 5: Results for different values of ε in Example 1 with $N_t = 20$. Uniform spaced nodes (left) and circular nodes (right), using Dirichlet and Neumann conditions.

ε	MAE	RMSE	L_{er}^1	MAE	RMSE	L_{er}^1
0.1	3.25E-04	6.79E-05	1.34E-04	3.90E-04	1.19E-04	2.76E-04
0.2	2.90E-04	5.54E-05	1.06E-04	3.79E-04	1.04E-04	2.36E-04
0.3	2.32E-04	3.69E-05	6.42E-05	3.61E-04	8.18E-05	1.74E-04
0.4	1.83E-04	3.11E-05	6.57E-05	3.36E-04	6.73E-05	1.35E-04
0.5	1.67E-04	6.63E-05	1.57E-04	3.61E-04	9.30E-05	1.86E-04
0.6	3.10E-04	1.25E-04	2.93E-04	5.38E-04	1.61E-04	3.46E-04
0.7	5.26E-04	2.02E-04	4.67E-04	7.90E-04	2.58E-04	5.69E-04

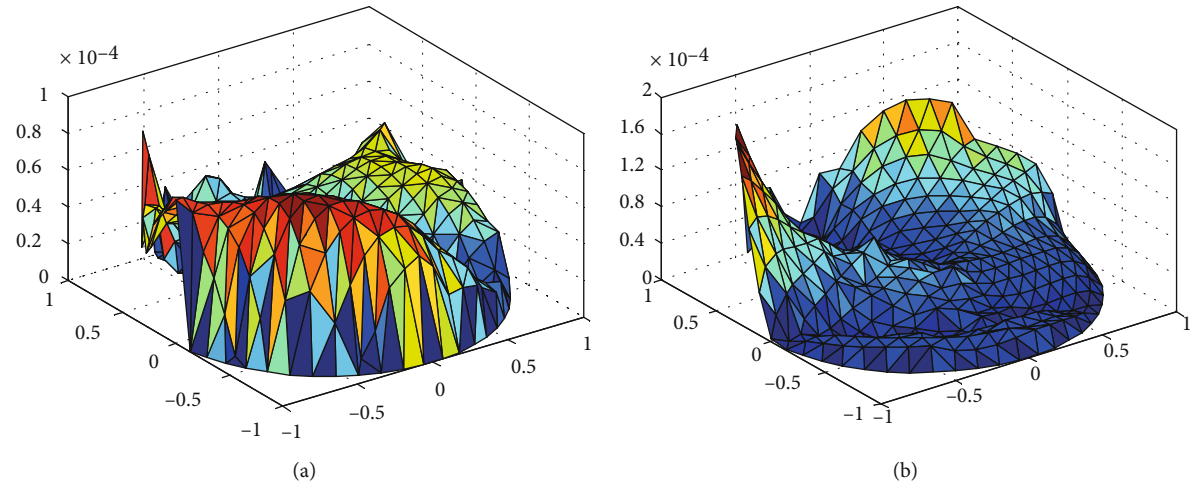

Figure 6: Absolute Errors at $t = 1$ with $N_t = 10$. Uniform (a) and circular (b). Example 1 using Dirichlet and Neumann conditions.

case, the number of neighboring points used is $n_s = 9$, if the collocation point considered belongs to the boundary of Neumann condition Γ_2 and $n_s = 7$ for the all other centers. Tables 4 and 5 present the results obtained for $N_t = 10$ and 20 for different distribution of nodes.

Figure 6 shows the maximum and root mean errors of the approximate solution at $t = 1$ for mixed boundary condition and different distributed nodes. Their values are MAE $= 8.55 \times 10^{-5}$ and RMSE $= 4.20 \times 10^{-5}$ for uniformly distributed collocation points using $\varepsilon = 0.47$. For the circular distributed nodes, we obtain MAE $= 1.78 \times 10^{-4}$ and RMSE $= 4.91 \times 10^{-5}$ for $\varepsilon = 0.43$. We can conclude that accurate results have been obtained for this first example.

Example 2. The second simulated case is the problem with the analytical solution represented by

$$u(x, y, t) = \frac{1}{2 - t} \exp\left(-\frac{x^2 + y^2}{2 - t}\right), \Omega \times [0, 1]. \quad (34)$$

where $a(x, y, t) = (1 + x^2)(2 - t)$ and $b(x, y, t) = xyt + 1$.

The computational domain and boundaries are the same as for Example 1. The simulation of this second example shows some difficulties compared to Example 1 because of the pseudosingularity that present at points with $t = 2$. Keeping the same neighboring points value $n_s = 7$, Tables 6 and 7

Table 6: Results for different values of ε in Example 2 with $N_t = 10$. Uniform spaced nodes (left) and circular nodes (right), with Dirichlet conditions.

ε	MAE	RMSE	L_{er}^1	MAE	RMSE	L_{er}^1
0.1	1.71E-03	2.99E-04	3.80E-04	7.25E-04	1.04E-04	1.14E-04
0.2	1.55E-03	2.52E-04	3.06E-04	5.67E-04	1.21E-04	1.41E-04
0.3	1.29E-03	1.78E-04	1.83E-04	8.37E-04	1.88E-04	2.55E-04
0.4	9.04E-04	1.12E-04	1.01E-04	1.23E-03	3.11E-04	4.54E-04
0.5	9.00E-04	1.94E-04	2.82E-04	1.76E-03	4.88E-04	7.31E-04
0.6	1.58E-03	3.95E-04	5.92E-04	2.46E-03	7.23E-04	1.09E-03
0.7	2.43E-03	6.64E-04	1.00E-03	3.34E-03	1.02E-03	1.55E-03

Table 7: Results for different values of ε in Example 2 with $N_t = 20$. Uniform spaced nodes (left) and circular nodes (right), with Dirichlet conditions.

ε	MAE	RMSE	L_{er}^1	MAE	RMSE	L_{er}^1
0.1	1.55E-03	3.46E-04	4.76E-04	5.66E-04	9.00E-05	1.15E-04
0.2	1.39E-03	2.98E-04	4.04E-04	3.97E-04	6.58E-05	8.62E-05
0.3	1.11E-03	2.17E-04	2.81E-04	4.02E-04	1.01E-04	1.47E-04
0.4	7.08E-04	1.04E-04	1.12E-04	6.63E-04	2.17E-04	3.43E-04
0.5	1.76E-04	8.89E-05	1.55E-04	1.11E-03	3.88E-04	6.14E-04
0.6	7.13E-04	2.87E-04	4.71E-04	1.74E-03	6.14E-04	9.67E-04
0.7	1.52E-03	5.49E-04	8.73E-04	2.56E-03	9.01E-04	1.42E-03

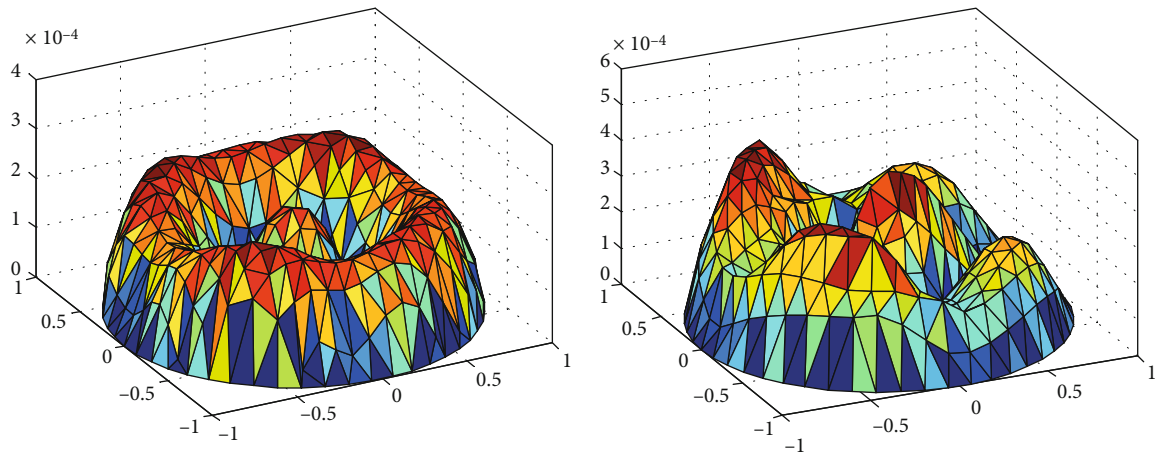

Figure 7: Absolute errors at $t = 1$ with $N_t = 10$. Uniform (a) and circular (b). Example 2 with Dirichlet conditions.

give obtained results for different value of N_t considering Dirichlet boundary condition.

From Figure 7, we can remark that at $t = 1$, we obtain MAE $= 2.51 \times 10^{-4}$ with $\varepsilon = 0.53$ for the uniform distributed nodes and MAE $= 4.13 \times 10^{-4}$ with $\varepsilon = 0.26$ for the circular distributed nodes.

Following the same step of simulation done before, Example 2 was then solved by considering mixed Neumann-Dirichlet boundary condition: Neumann condition on Γ_2 and Dirichlet conditions on Γ_1. On the boundary with the Neumann condition, the number of selected neighboring point is set to be $n_s = 9$. Tables 8 and 9 give the found results found.

Example 3. The investigated problem is the widely used convection-diffusion flow problem of a Gaussian pulse given by the equation:

$$\frac{\partial u}{\partial t}(x, y, t) + \mathrm{v}(x, y, t)\nabla u(x, y, t) - \nu \Delta u(x, y, t) = f(x, y, t) \forall (x, y, t) \in \Omega \times]0, T], \tag{35}$$

Table 8: Results for different values of ε in Example 2 with $N_t = 10$. Uniform spaced nodes (left) and circular nodes (right), with Neumann conditions.

ε	MAE	RMSE	L_{er}^1	MAE	RMSE	L_{er}^1
0.1	1.72E-03	3.29E-04	4.53E-04	1.19E-03	2.07E-04	2.92E-04
0.2	1.51E-03	2.71E-04	3.59E-04	1.43E-03	1.91E-04	2.33E-04
0.3	1.42E-03	2.39E-04	2.95E-04	1.85E-03	3.09E-04	3.91E-04
0.4	1.85E-03	3.67E-04	4.88E-04	2.46E-03	5.87E-04	8.68E-04
0.5	2.44E-03	6.59E-04	9.97E-04	3.29E-03	9.97E-04	1.55E-03
0.6	3.23E-03	1.08E-03	1.71E-03	4.37E-03	1.54E-03	2.45E-03
0.7	4.23E-03	1.63E-03	2.63E-03	5.76E-03	2.24E-03	3.58E-03

Table 9: Results for different values of ε in Example 2 with $N_t = 20$. Uniform spaced nodes (left) and circular nodes (right), with Neumann conditions.

ε	MAE	RMSE	L_{er}^1	MAE	RMSE	L_{er}^1
0.1	1.61E-03	3.93E-04	5.79E-04	8.84E-04	2.48E-04	3.81E-04
0.2	1.39E-03	3.21E-04	4.64E-04	1.11E-03	1.69E-04	2.43E-04
0.3	1.08E-03	2.30E-04	3.28E-04	1.51E-03	1.89E-04	2.24E-04
0.4	1.47E-03	2.61E-04	3.25E-04	2.09E-03	4.39E-04	6.63E-04
0.5	2.03E-03	5.11E-04	7.80E-04	2.88E-03	8.30E-04	1.33E-03
0.6	2.76E-03	9.03E-04	1.47E-03	3.90E-03	1.35E-03	2.18E-03
0.7	3.70E-03	1.41E-03	2.32E-03	5.20E-03	1.99E-03	3.21E-03

where $\mathrm{v}(x, y, t) = (-4y, 4x)^T$ is the velocity vector, and ν is a constant. Initial and boundary conditions are taken according to the analytical solution:

$$u(x, y, t) = \frac{\sigma^2}{\sigma^2 + 4\nu t} \exp\left(-\frac{(x-0.5)^2 + (y-0.5)^2}{\sigma^2 + 4\nu t}\right). \quad (36)$$

In our simulation, we take $\sigma^2 = 0.001$ and $\nu = 0.01$. The computational space-time domain Ω_T is $[0, 1] \times [0, 1] \times [0, \pi/2]$. In Figure 8, we show the numerical solution at final time $t = T$ face to the analytical solution, the total number of nodes is $N = 30^3$. Table 10 displays the absolute maximum error obtained for different values of N; it can be remarked that the rate of convergence is near quadric. In all simulations for Example 3, the shape parameter is chosen to be $\varepsilon = 5$.

3.3. Two-Dimensional Hyperbolic Equations. Although it has been shown that the technique gives good results solving the parabolic equation with different boundary conditions, the hyperbolic equation is still an important and interesting equation to be tested using the described methodology. In all simulations, the problem is treated as an ill-posed one as it has mentioned before and the algebraic matrix obtained is square.

Example 4. Considering a two-dimensional wave problem defined by the following equation on the domain $\Omega \times]0, T[$ with $\Omega = [0, 1]^2$

$$\frac{\partial^2 u}{\partial t^2}(x, y, t) - a\Delta u(x, y, t) = f(x, y, t) \forall (x, y, t) \in \Omega \times]0, T], \quad (37)$$

with two initial conditions $u(x, 0) = u_0(x)$ and $\partial u/\partial t(x, y, 0) = h(x, y)$ and Dirichlet boundary condition on $\partial\Omega$.

Taking $a(x, y, t) = xye^{-2t}$, the functions u_0, h, and f are chosen according to the analytical solution given by $u(x, t) = \sin x \sin y \sin t$.

Applying the "ill-posed-problem" technique [22], we obtain accurate results by setting the number of neighboring points to be $n_s = 9$ in the entire domain. Table 11 shows results obtained of different errors, taking $\varepsilon = 0.1$ and using the space-time domain $]0, 1[^3$. Figure 9 shows that the MAE error decreases when increasing the number of nodes.

As in the example of the one-dimensional problem, the convergence rate of the technique using different uniformly distributed sources points and $\varepsilon = 0.1$ is given in Table 12 showing that the order of convergence is quadratic.

At $t = 1$, the maximum absolute error is $\mathrm{MAE} = 6.68 \times 10^{-5}$, and the root mean square error is $\mathrm{RMSE} = 1.81 \times 10^{-5}$; these values are obtained with $\varepsilon = 0.1$ and $N = 25^3$. We remark that the maximum error is obtained at $t = T$ (see Figure 10).

3.4. Three-Dimensional Parabolic and Hyperbolic Examples. In this section, we show the robustness and the accuracy of the proposed method implemented in high dimension problems. The traditional three-dimensional problems are transformed into 4D problems.

Example 5. The problem investigated is the 3D heat transfer problem given by the equation:

$$\frac{\partial u}{\partial t}(x, y, z, t) - a(x, y, z, t)\Delta u(x, y, z, t) = f(x, y, z, t). \quad (38)$$

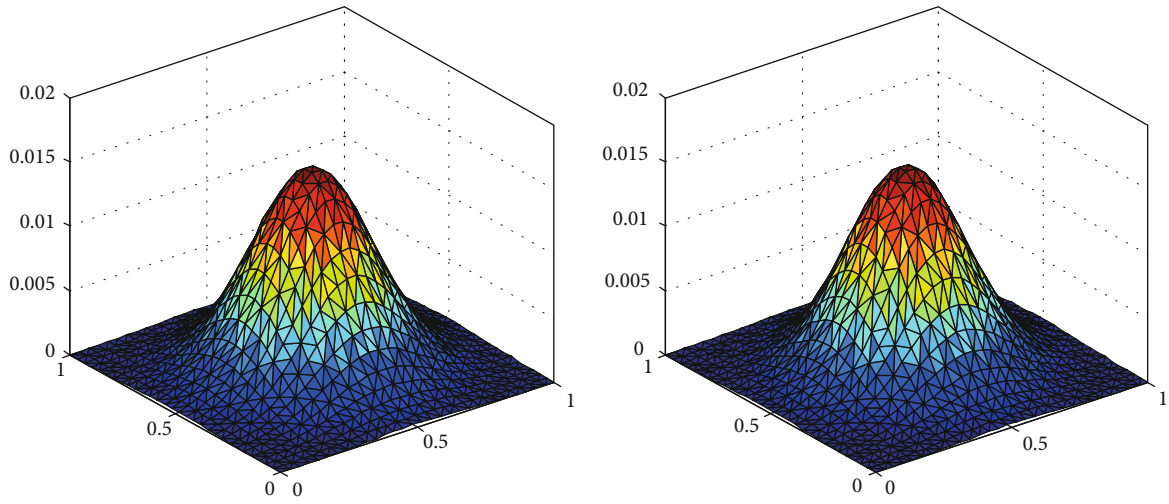

Figure 8: Exact (a) and numerical (b) solutions at $t = \pi/2$ for the Example 3 with $N = 30^3$ and $\varepsilon = 5$.

Table 10: Maximum absolute error and rate of convergence at $t = T$ for different values of N in Example 3 using $\varepsilon = 5$ and $\Omega_T = [0, 1] \times [0, 1] \times [0, \pi/2]$.

N	MAE	h	ROC
15^3	6.70E-04	0.0714	—
20^3	3.74E-04	0.0526	1.91
25^3	2.35E-04	0.0417	1.99
30^3	1.62E-04	0.0345	1.96

With $a(x, y, z, t) = xyze^t$, the initial and boundary conditions are chosen in such a way that the analytical solution is given by the function $u(x, y, z, t) = e^{-t} \sin x \sin y \sin z$. The space-time domain is chosen $\Omega =]0, 1[^4$ and the right-hand side is $f(x, y, z, t) = \sin(x) \sin(y) \sin(z) e^{-t}(-1 + 3xyze^t)$.

Taking $n_s = 9$, Table 13 shows the errors found in two simulations. The total number of nodes is $N = N_x \times N_t \times N_y \times N_z = 5^4$ and $N = 9^4$.

We can remark that good accuracy is obtained even with weak number of nodes. We note that similar accuracy is found using different values of the shape parameter ε in the interval [0,1.5]

Example 6. The considered hyperbolic 3D problem is given by

$$\frac{\partial^2 u}{\partial t^2}(x, y, z, t) - a(x, y, z, y, t)\Delta u(x, y, z, t) = f(x, y, z, t). \tag{39}$$

We use $a(x, y, z, t) = xyze^{-t}$ and $\varepsilon = 0.12$. The computational space-time domain is $\Omega =]0, 1[^4$. The boundary and initial conditions and the function f are chosen according to the solution $u(x, y, z, t) = \sin x \sin y \sin z \sin t$. In this example, the number of neighboring points is set to $n_s = 11$ on the entire domain. The total number of nodes is $N = N_x \times N_t \times N_y \times N_z = 9^4$. The errors obtained for this example are MAE $= 1.54 \times 10^{-3}$, RMSE $= 9.23 \times 10^{-5}$, and $L_{er}^1 = 6.00 \times 10^{-4}$. The same ill-posed technique is used with the squared algebraic linear system.

Table 11: Errors for different values of N_x, N_y, and N_t of Example 4 using $\varepsilon = 0.1$ and $\Omega_T = [0, 1]^3$.

N_x	N_y	N_t	MAE	RMSE	L_{er}^1
5	5	5	1.80E-03	5.13E-04	2.69E-03
10	10	10	4.59E-04	1.26E-04	8.08E-04
15	15	15	1.91E-04	5.23E-05	3.53E-04
20	20	20	1.06E-04	2.86E-05	1.97E-04
25	25	25	6.68E-05	1.81E-05	1.25E-04

4. Conclusion

The local space-time RBF collocation method developed in [13] is extended to solve parabolic and hyperbolic equations with variable coefficients in the space-time domain. Following the same technique used in [13], the parabolic problem is solved using the governing equation as boundary condition on the boundary characterized by the final time T, and the hyperbolic equation is solved as an ill-posed problem with incomplete data boundary condition on $\Omega \times \{t = T\}$. The first one-dimensional tested numerical simulation concerns the comparison of the 4th order Runge-Kutta method to the presented one. It has been shown that although the Runge-Kutta method did not need the inversion of the matrix and it is considered as an explicit technique, it needs more CPU time than the proposed one.

The numerical results obtained for other two- and three-dimensional parabolic and hyperbolic problems show the performance of the technique and its accuracy for solving different examples. It has been demonstrated that the technique is simple, straightforward. The formulation of the hyperbolic

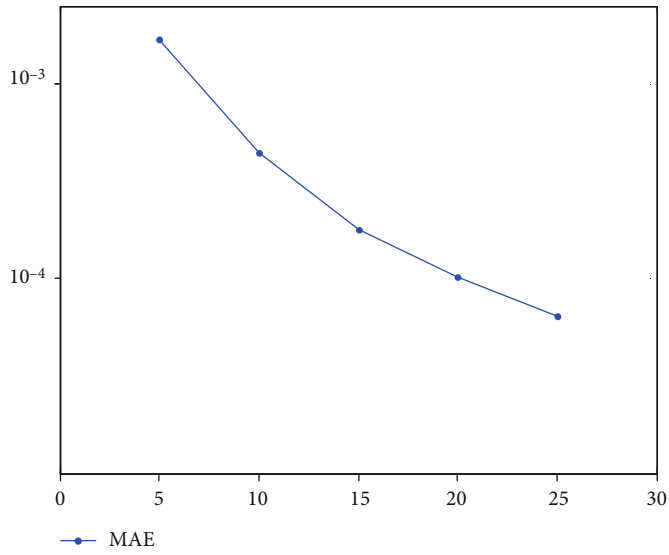

Figure 9: Maximum absolute errors vs. N_x with $N_x = N_y = N_t$ of Example 4 using $\varepsilon = 0.1$.

Table 12: Rate of convergence for wave Example 4 using $\varepsilon = 0.1$.

h	MAE	ROC	RMSE	ROC	L^1_{er}	ROC
0.25000	1.70E-03	—	4.61E-04	—	2.44E-03	—
0.11111	4.46E-04	1.6460	1.22E-04	1.6363	7.86E-04	1.3970
0.07143	1.78E-04	2.0796	4.92E-05	2.0596	3.34E-04	1.9365
0.05263	1.02E-04	1.8190	2.80E-05	1.8516	1.94E-04	1.7833
0.04167	6.43E-05	1.9835	1.78E-05	1.9383	1.25E-04	1.8771

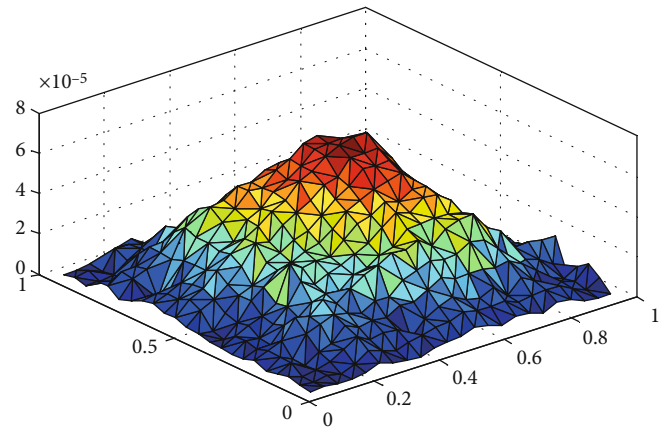

Figure 10: Absolute errors with $N_t = 25$ and $\varepsilon = 0.1$ at $t = 1$, for Example 4.

Table 13: Errors for Example 5 using two different values of N.

N	ε	MAE	RMSE	L^1_{er}
5^4	0.9	4.88E-4	9.28E-5	5.45E-4
9^4	0.8	2.23E-4	3.62E-5	2.75E-4

equation as an ill-posed problem and also its application to three-dimensional problems and quasisingular problems with variables coefficients are the most important ideas of the paper. We can also remark that the main advantages of the technique which are

(1) The time stability analysis is not discussed as it is the case for other time-stepping algorithms as implicit, explicit, θ-method, etc.

(2) Reducing the computational time as there is no need to recompute the matrix for the resulting algebraic system at each time level, unlike the case for other

time integration methods used to solve PDEs with time-dependent coefficients and

(3) Solving hyperbolic partial differential equations with variable coefficients as an inverse problem, since just the hyperbolic equation with constant coefficients is less discussed and needs more sophisticated time integration technique

are more representative for partial differential equation with variable coefficients than with constant one. Further work will focus on the application of the developed technique to nonlinear equations. Stability analysis of the technique should also be investigated in further work.

5. Further Work

Further work will focus on applying the method to more real PDEs like the equation of the telegraph and the transient heat conduction problem in an anisotropic medium, all this PDEs will be investigated with variable coefficients.

Data Availability

The data used to support the study is available within the article.

Conflicts of Interest

The authors declare that they have no conflicts of interest

References

[1] F. Parzlivand and A. M. Shahrezaee, "Numerical solution of an inverse reaction-diffusion problem via collocation method based on radial basis functions," *Applied Mathematical Modelling*, vol. 39, no. 13, pp. 3733–3744, 2015.

[2] M. Dehghan and A. Shokri, "A meshless method for numerical solution of a linear hyperbolic equation with variable coefficients in two space dimensions," *Numerical Methods for Partial Differential Equations*, vol. 25, no. 2, pp. 494–506, 2009.

[3] T. Jiang, M. Li, and C. S. Chen, "The method of particular solutions for solving inverse problems of a nonhomogeneous convection-diffusion equation with variable coefficients," *Numerical Heat Transfer, Part A*, vol. 61, no. 5, pp. 338–352, 2012.

[4] C. M. Fan, C. S. Chen, and J. Monroe, "The method of fundamental solutions for solving convection-diffusion equations with variable coefficients," *Advances in Applied Mathematics and Mechanics*, vol. 1, pp. 215–230, 2009.

[5] L. Ming, C. S. Chen, and C. H. Tsai, "Meshless method based on radial basis functions for solving parabolic partial differential equations with variable coefficients," *Numerical Heat Transfer, Part B: Fundamentals*, vol. 57, pp. 333–347, 2010.

[6] C. S. Chen, C. M. Fan, and P. H. Wen, "The method of APPROXIMATE particular solutions for solving elliptic problems with variable coefficients," *International Journal of Computational Methods*, vol. 8, no. 3, pp. 545–559, 2011.

[7] G. Yan, Q. Hua, C. Zhang, and X. He, "The generalized finite difference method for long-time transient heat conduction in 3D anisotropic composite materials," *Applied Mathematical Modelling*, vol. 71, pp. 316–330, 2019.

[8] Y. Gu and H. Sun, "A meshless method for solving three-dimensional time fractional diffusion equation with variable-order derivatives," *Applied Mathematical Modelling*, vol. 78, pp. 539–549, 2020.

[9] T. E. Tezduyar, S. Sathe, R. Keedy, and K. Stein, "Space-time finite element techniques for computation of fluid-structure interactions," *Comput Methods Appl Mech Eng*, vol. 195, no. 17-18, pp. 2002–2027, 2006.

[10] C. M. Klaij, J. J. W. van der Vegt, and H. van der Ven, "Space-time discontinuous Galerkin method for the compressible Navier-Stokes equations," *Journal of Computational Physics*, vol. 217, no. 2, pp. 589–611, 2006.

[11] J. J. Sudirham, J. J. W. van der Vegt, and R. M. J. van Damme, "Space-time discontinuous Galerkin method for advection-diffusion problems on time-dependent domains," *Applied Numerical Mathematics*, vol. 56, no. 12, pp. 1491–1518, 2006.

[12] V. R. Ambati and O. Bokhove, "Space-time discontinuous Galerkin finite element method for shallow water flows," *Journal of Computational and Applied Mathematics*, vol. 204, no. 2, pp. 452–462, 2007.

[13] M. Hamaidi, A. Naji, and A. Charafi, "Space-time localized radial basis function collocation method for solving parabolic and hyperbolic equations," *Engineering Analysis with Boundary Elements*, vol. 67, pp. 152–163, 2016.

[14] Z. Li and X. Z. Mao, "Global space-time multiquadric method for inverse heat conduction problem," *International Journal for Numerical Methods in Engineering*, vol. 85, no. 3, pp. 355–379, 2011.

[15] Z. Li and X. Z. Mao, "Global multiquadric collocation method for groundwater contaminant source identification," *Environmental Modelling & Software*, vol. 26, no. 12, pp. 1611–1621, 2011.

[16] T. S. Li and S. M. Wong, "Development of an efficient and accurate global space-time radial basis collocation model for estimation of river pollution source," *IACSIT International Journal of Engineering and Technology*, vol. 6, no. 2, 2014.

[17] H. Netuzhylov, *A space-time meshfree collocation method for coupled problems on irregularly-shaped domains, [PhD thesis]*, TU Braunschweig, CSE-Computational Sciences in Engineering, 2008.

[18] D. E. Myers, S. De Iaco, D. Posa, and L. De Cesare, "Space-time radial basis functions," *Computers and Mathematics with Applications*, vol. 43, no. 3-5, pp. 539–549, 2002.

[19] H. Wendland, *Scattered Data Approximation*, Cambridge University Press, 2005.

[20] M. Li, W. Chen, and C. S. Chen, "The localized RBFs collocation methods for solving high dimensional PDEs," *Engineering Analysis with Boundary Elements*, vol. 37, no. 10, pp. 1300–1304, 2013.

[21] G. Yao, J. Kolibal, and C. S. Chen, "A localized approach for the method of approximate particular solutions," *Computers and Mathematics with Applications*, vol. 61, no. 9, pp. 2376–2387, 2011.

[22] M. Hamaidi, A. Naji, F. Ghafrani, and M. Jourhmane, "Noniterative localized and space-time localized RBF meshless method to solve the ill-posed and inverse problem," *Modelling and Simulation in Engineering*, vol. 2020, Article ID 5046286, 2020.